PAPER

Effect of swift heavy ion irradiation on $Zr_{70}Ni_{30}$ binary metallic glass: a positron annihilation study

Physica Scripta

PAPER

RECEIVED
1 December 2025

REVISED
13 March 2026

ACCEPTED FOR PUBLICATION
1 April 2026

PUBLISHED
16 April 2026

Effect of swift heavy ion irradiation on $Zr_{70}Ni_{30}$ binary metallic glass: a positron annihilation study

Wafa Boukhemkhem[1,*], Rafik Hazem[2], Mahmoud Izerrouken[3,†], Matteo Ghidelli[4], Thomas Pardoen[5,6], Saygin Kuzeci[7], Murat Yavuz Yener[8], Cumali Tav[9] and Ugur Yahsi[9]

[1] Laboratory of Research on the Physico-Chemistry of Surfaces and Interfaces (LRPCSI), University of 20 August 1955-Skikda, BP 26, 21000 Skikda, Algeria
[2] Laboratory of Coating, Materials and Environment, University M'Hamed Bougara Boumerdes, 35000, Boumerdes, Algeria
[3] Nuclear Research Center of Draria, BP 43, Sebbala, Draria, Algiers, Algeria
[4] Laboratoire des Sciences des Procédés et des Matériaux (LSPM), CNRS, Université Sorbonne Paris Nord, 93430, Villetaneuse, France
[5] Institute of Mechanics, Materials and Civil Engineering, UCLouvain, Place Sainte-Barbe 2, 1348 Louvain-la-Neuve, Belgium
[6] WEL Research Institute, Avenue Pasteur 6, 1300 Wavre, Belgium
[7] Physics Department, College of Education for Pure Science, Kirkuk University, 36001 Kirkuk, Iraq
[8] BETAM, Fatih Sultan Mehmet Vakif University Topkapi Campus, Zeytinburnu, Istanbul, Turkey
[9] Department of Physics, Faculty of Science, Marmara University, 34722, Kadikoy, Istanbul, Turkey
[†] We dedicate this paper to the memory of the late Professor Izerrouken Mahmoud (Senior Researcher, CRND), who served as the principal coordinator of this research prior to his passing on November 22, 2025. He was an outstanding and a highly respected scientist. His dedication to research and his pioneering contributions to the field will continue to inspire us.
[*] Author to whom any correspondence should be addressed.

E-mail: w.boukhemkhem@univ-skikda.dz

Keywords: $Zr_{70}Ni_{30}$ binary metallic glass, heavy-ion irradiation, free volume, positron annihilation spectroscopy

Abstract

The assessment of irradiation effects in metallic glasses is important considering the renewed interest for this class of material for a variety of nuclear applications. The $Zr_{70}Ni_{30}$ thin films metallic glass (MG) deposited on Si substrate by magnetron sputtering technique were exposed to 93.2MeV $^{129}Xe^{23+}$ heavy-ion irradiation at room temperature, covering a range of ion fluences from 5×10^{12}ionscm^{-2} to 8×10^{13}ionscm^{-2}. The evolution of the irradiation-induced defects in $Zr_{70}Ni_{30}$ MG has been investigated using Doppler broadening spectroscopy (DBS) and positron annihilation lifetime spectroscopy (PALS). Three lifetime components were distinguished, indicating the presence of different types of open-volume regions at the atomic scale in thin film. The combined results of both DBS and PALS demonstrated that ion irradiation initially increases the excess free-volume density with a homogeneous distribution up to a fluence of ($\leqslant2\times10^{13}$ionscm^{-2}). In contrast, with increasing fluence ($>2\times10^{13}$ionscm^{-2}), a reduction in excess free-volume was found, which could be related to structural relaxation accompanied by modifications in atomic arrangement and defect distribution. Moreover, the correlation between the shape and wing parameters provides a basis to identify the nature of the defects, indicating that the type of defect changes at the higher fluence of 4×10^{13}ionscm^{-2} and 8×10^{13}ionscm^{-2}, which affects the performance of $Zr_{70}Ni_{30}$ metallic glass after ion irradiation.

1. Introduction

Metallic glasses are considered as promising structural candidates for nuclear reactors due to their high resistance to irradiation damage. However, the formation and evolution of defects at the atomic level under irradiation needs to be studied more thoroughly before application in harsh operating conditions of nuclear reactors [1, 2]. These environments, characterized by high radiation damage levels extended to 100 displacements per atom (dpa), elevated temperatures changing between 300 °C to 700 °C, and contact with corrosive substances, control the durability and degradation of structural nuclear materials. The selection of a material is based on its specific properties with respect to the constraints induced by these environmental

factors, which vary as a function of the position in the reactor core [3]. Zr-based alloys, in particular, exhibit a very low thermal neutron absorption coefficient and excellent corrosion resistance [4]. Accordingly, these alloys are considered the most prevalent fuel rod cladding material, especially in light-water reactors (LWRs).

With the continuous advancement of nuclear technology, there is pressure to keep improving accident-tolerance of Zr alloy fuel claddings through several strategies proposed in the literature, such as (i) enhancing the Zr alloy cladding's oxidation resistance by applying suitable coatings, (ii) using alternative cladding materials that show outstanding performance compared to Zr alloys, (iii) introducing appropriate fuel systems that show better thermal conductivity [5]. Numerous researchers have focused on coating layers as thin protective surfaces to improve corrosion or oxidation resistance [6, 7]. Thin film metallic glasses (TFMGs) have emerged as one of the suitable coating materials in nuclear structural applications [8]. Specifically, metallic glasses (MGs) are characterized by a structure with atomic disorder and the absence of crystalline defects (for example, grain boundaries and dislocations), which are ubiquitous in crystalline materials. This structure is responsible for the salient mechanical characteristics, including a significant yield strength (up to 2 GPa), high hardness (ranging from 5 to 10 GPa), and relatively high fracture toughness in comparison with their crystalline counterparts [9, 10].

To understand the behavior and performance of metallic glasses (MGs) in nuclear facilities, different types of particles, such as neutrons [2], electrons [11], and ions [12, 13] have been used in both experimental and simulation studies. Irradiation has been demonstrated to significantly enhance the corrosion resistance of MGs [14], which provides further motivation for application in irradiated environments [15]. For example, Huang *et al* [16] investigated the corrosion behavior of Fe-based metallic glass and demonstrated its performance for applying in nuclear waste environments to store spent nuclear fuel.

According to the literature, radiation induces different types of defects in amorphous alloys. Petrusenko *et al* [17] reported the creation of vacancy-like and interstitial-like defects, corresponding to density fluctuations created along ion tracks in metallic glasses under electron irradiation (E_e=2.5MeV). At the atomic scale, irradiation in metallic glasses generates excess free volume, thereby reducing the atomic packing density. This excess free volume is referred to as free volume in much of the literature. The free volume is commonly defined as the surplus atomic volume relative to an ideal dense, disordered structure [18]. While both terms are often used interchangeably, 'free volume' applies strictly to specific free-volume models. In this work, to avoid ambiguity, we designate the additional volume as excess free volume, consistent with our positron annihilation spectroscopy analysis. Depending on the irradiation conditions, the excess free volume in metallic glasses can either increase or decrease: in the case of an increase, structural rejuvenation is promoted and softening may occur, whereas a decrease enhances structural relaxation and may lead to hardening [19, 20]. Molecular dynamics simulations further suggest that, unlike crystalline materials, amorphous metallic glasses exhibit a self-healing process in their internal microstructure [2]. High-resolution transmission electron microscopy (HRTEM) observations have also shown that irradiation with 2MeV electrons induces nanocrystallization and the formation of nanocrystalline phases in $Zr_{66.7}Cu_{33.3}$ and $Zr_{66.7}Pd_{33.3}$ metallic glasses (MGs) [21].

Overall, irradiation-induced modifications in the atomic structure are directly linked to changes in the functional properties of MGs, including their mechanical and chemical behavior. Understanding these defects at the atomic scale is therefore essential for predicting the performance of MGs in practical applications. Such effects are typically characterized using several techniques, including transmission electron microscopy (TEM), atom probe spectroscopy for compositional analysis, and positron annihilation spectroscopy (PAS). The latter has been widely used and remains the best technique for probing open-volume defects (void spaces) as well as their associated chemical environments [22].

The positron annihilation lifetime spectroscopy measurements revealed a substantial concentration of vacancy-like defects in Hf–Nb–Ta–Ti–Zr high-entropy amorphous films [23]. A study by Onodera *et al* [13] demonstrated that irradiation with 10MeV I^{3+} ions produced no significant change in the coincidence Doppler broadening (CDB) ratio of the $Zr_{50}Cu_{40}Al_{10}$ metallic glass, suggesting the absence of long-range atomic reordering. However, a reduction in positron lifetime was also observed under all irradiation conditions, indicating a decrease in excess free volume, which is linked to inelastic collisions with electrons throughout irradiation. According to Fukumoto *et al* [24], positron lifetime of ZrCuAl MG increased after electron irradiation (E_e=2MeV), indicating an enlargement of the excess free volume without affecting the atomic arrangement. whereas, Xe-ion irradiation (E_{Xe}=200 MeV) caused a decrease in positron lifetimes, suggesting that the excess free volume is reduced and the amorphous structure is maintained after ion irradiation.

Nevertheless, limited experimental studies are available for Zr-based systems under irradiation, particularly those conducted using positron annihilation spectroscopy (see [13, 25, 26] and the references therein), motivating the present study. The Zr-Ni system serves as a model binary alloy to investigate irradiation effects because of its high glass-forming ability (GFA) with different compositions as well as its well-reported structural properties in the literature. Particularly $Zr_{70}Ni_{30}$ metallic glass was selected for its proximity to the amorphization boundary and exhibiting good mechanical properties, like hardness and strength, as previously reported [27].

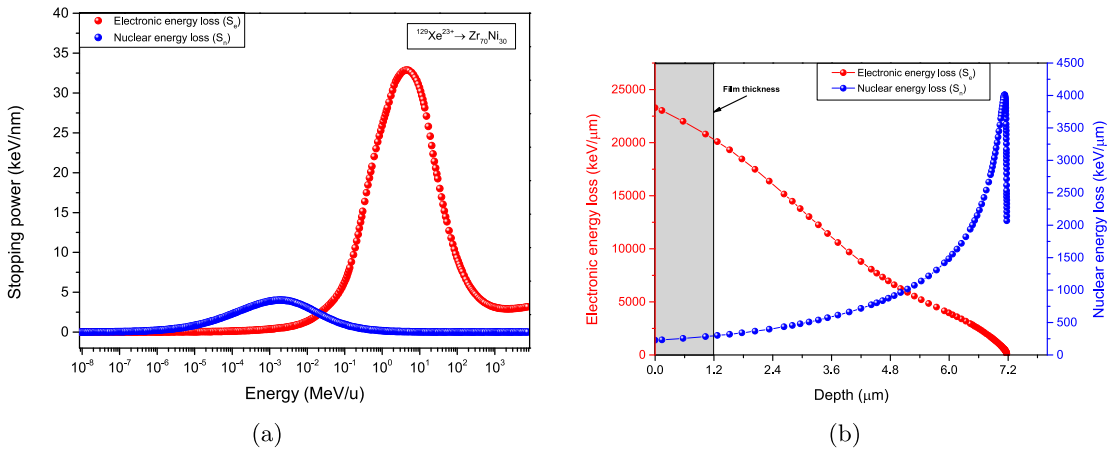

Figure 1. Distribution of electronic energy loss (S_e) and nuclear energy loss (S_n) as a function of (a) incident Xe ion energy and (b) the penetration depth in $Zr_{70}Ni_{30}$ metallic glass. The shaded area in the plot indicates the film thickness.

This research studies the evolution of ion irradiation-induced defects in binary Zr-Ni metallic glass using the PAS technique. This latter is sensitive to microscopic open-volume defects, and has high detection precision. We primarily focus on the analysis of the Doppler broadening spectroscopy (DBS) depth profile, while the positron annihilation lifetime spectroscopy (PALS) data provides supporting information to complement our findings. The goal is to highlight the impact of a range of ion fluences on defect formation and evolution, as reflected by variation in DBS and PALS characteristics. This investigation extends the previous research [28], which reported that heavy-ion irradiation can induce surface smoothening, leading to enhanced corrosion resistance and a complex variation of the hardness.

2. Materials and methods

2.1. Material and sample preparation

$Zr_{70}Ni_{30}$, TFMG with an average thickness equal to ≈1.2μm, was deposited onto a monocrystalline Si substrate by magnetron sputtering. The sputtering technique was performed using a suitable target of 99.99 % pure Zr and 99.95 % pure Ni. Additional details on the sample preparation are available in previous work [29].

2.2. Irradiation experiments

The heavy-ion irradiation experiment was performed at the GANIL (Grand Accélérateur National d'Ions Lourds) laboratory by employing the IRRSUD (IRRadiation SUD) experimental line at room temperature. The $Zr_{70}Ni_{30}$ metallic glass films were subjected to 93.2MeV $^{129}Xe^{23+}$ heavy-ions irradiation over a range of ion fluences from 5×10^{12} ions cm^{-2} to 8×10^{13} ions cm^{-2}. Part of the five samples was masked with aluminum sheets, which served as a reference for comparison with the irradiated regions. A simulation with the SRIM (Stopping and Range of Ions in Matter) software [30] indicates that the interaction of Xe-ions with $Zr_{70}Ni_{30}$ MG is predominantly governed by electronic energy losses (S_e), consequently, the energy transfer mainly occurs through inelastic collisions (see figures 1(a) and (b)).

The TRIM simulation results were determined using the SRIM software relying on detailed calculation with full damage cascades for 10,000 incidents ions. As illustrated in figures 2(a),–(d), the mean projected range Xe ions is approximately 7.1 μm. In addition, the total damage induced during the collision cascade is mostly attributed to vacancy creation (78,749 vacancies per ion) then the replacement collisions (1,808 events per ion) occurring in the $Zr_{70}Ni_{30}$ target. During irradiation, a small proportion of Xe ions directly interact with lattice sites, whereas the most prominent interactions occur with the target electrons of the thin film, indicating that most of incident ion energy is dissipated through the ionization mechanism. These results demonstrate that electronic energy loss (S_e) is the primary process responsible to irradiation-induced defects in the $Zr_{70}Ni_{30}$ thin film.

2.3. Positron annihilation techniques

The positron annihilation techniques are non-destructive processes that probe the open structures of solid materials, including both crystalline [31] and amorphous systems [32]. In particular, positron annihilation lifetime spectroscopy (PALS) is a direct technique for characterizing free volume. In this study, PALS measurements were performed using a fast-fast coincidence system, which determines the time interval

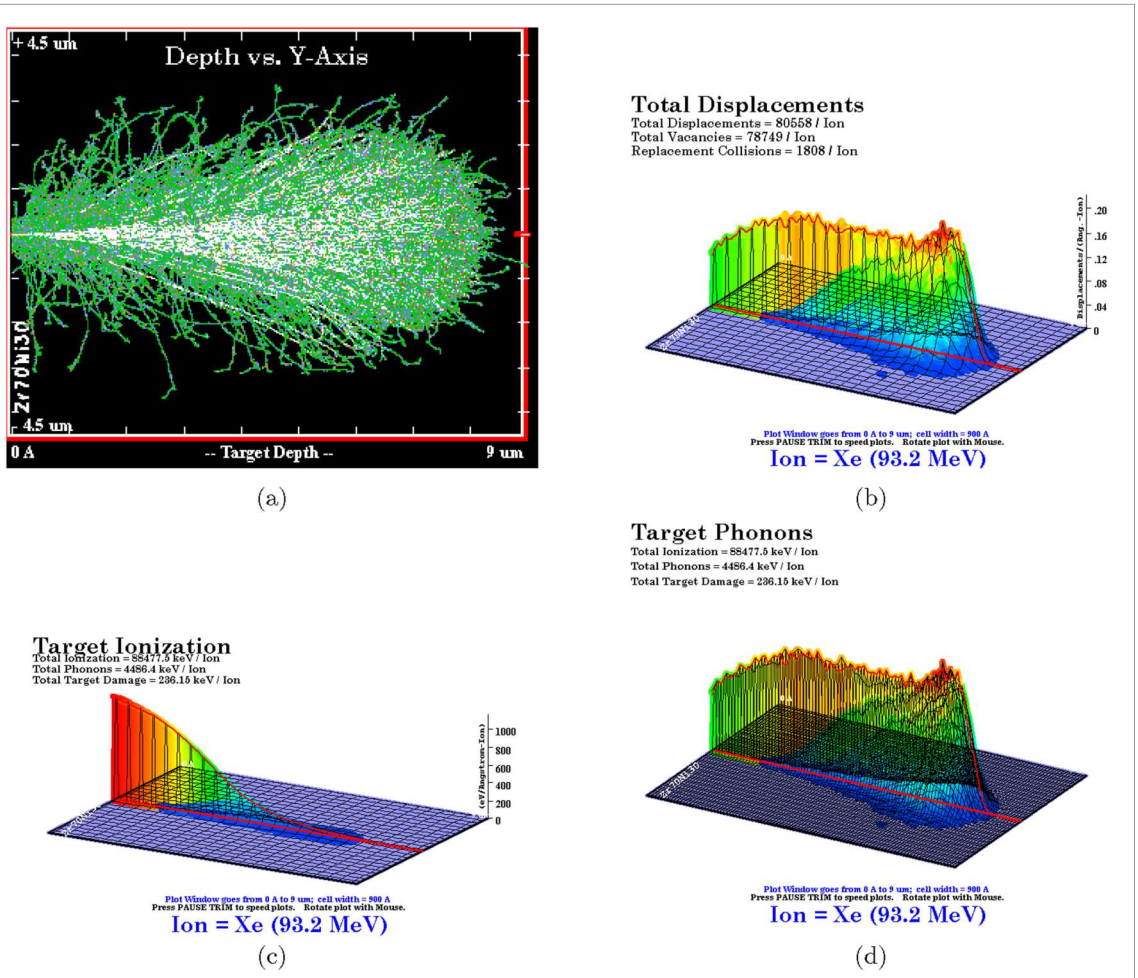

Figure 2. TRIM simulation results for 93.2MeV Xe ion irradiation of the $Zr_{70}Ni_{30}$ thin film (a) Schematic representation of the 2D view of Xe ions trajectories at Y-axis passing through the target material, and 3D views of (b) total damage, (c) target ionization, and (d) target phonons induced during irradiation, as determined using the SRIM code.

between two γ-rays: the γ-ray of 1274 keV serves as the start signal and is accompanied by positron emission, and the γ-ray of 511keV, produced by positron annihilation, indicates the stop signal. The positron source was prepared by depositing a solution of about μCi of ^{22}NaCl on a thin aluminum foil (5 μm thick), which was then sandwiched between two samples. Only one film sample was used per measurement; however, the measurements were repeated to obtain accurate statistical data for each irradiation fluence. One side consisted of the covered film, while the other side was the silicon (Si) substrate. Positrons emitted from the source (^{22}NaCl encapsulated in Kapton) have an energy spectrum ranging from zero up to 546keV, with an average energy of approximately 182keV. The low energy positrons around 29keV, primarily annihilate within the thin films, while the high energy positrons penetrate through the metallic glass $Zr_{70}Ni_{30}$ and implant into the underlying silicon substrate.

For the γ-ray detection, a plastic scintillator (BC422, Saint-Gobain Crystals, Ohio, USA) coupled to the photomultiplier tubes (PMT R2059, Hamamatsu Photonics Deutschland GmbH, Herrsching, Germany) mounted on a PMT Base (265A, Ortec AMETEK GmbH, Meerbusch, Germany) operating at negative 2010 volts was used. Two constant fractional differential discriminators (CFDD 583B, Ortec AMETEK GmbH, Meerbusch, Germany) were used for the window settings of 1274keV and 511keV and for generating timing signals. A time-to-amplitude converter (TAC 266, Ortec AMETEK GmbH, Meerbusch, Germany) was used to convert pulses of different heights into a time-to-pulse-height signal. The converted signals were then fed to a multichannel analyzer (Ethernim MCA 919E, Ortec AMETEK GmbH, Meerbusch, Germany). The spectroscopic data obtained from MCA were analyzed using the LT-92.3 software [33] to specify the lifetime and intensity. The system's resolution was around 320 ps, and a million counts were recorded at each PALS measurement.

In addition, Doppler broadening spectroscopy (DBS) has been conducted. This positron technique is based on the Doppler broadening of the annihilation gamma; it offers valuable insights into the momentum distribution of the annihilated electron-positron couples. When a positron comes into contact with an electron in a

material, the momentum of the combined positron-electron system in the annihilation direction is transmitted to the 511keV gamma line from annihilation, causing it to broaden due to the Doppler shift [34, 35]. The Doppler broadening spectrum can be divided into five distinct parts, focusing on the center and wing parts. The sharpness (S) and wing (W) parameters are defined as the fractions of counts in the central and wing regions of the Doppler-broadened annihilation peak relative to the total area of the peak [34, 35]. They are calculated using the following relations:

$$S = \frac{\int_{\Delta E_c} N(E)\,dE}{\int_{\Delta E_T} N(E)\,dE} \quad \text{and} \quad W = \frac{\int_{\Delta E_{Wleft}} N(E)\,dE + \int_{\Delta E_{Wright}} N(E)\,dE}{\int_{\Delta E_T} N(E)\,dE}$$

Where $N(E)$ is the number of counts at energy E, ΔE_c defines the central low-momentum window around the 511keV peak, and ΔE_T corresponds to the total integration window of the annihilation peak.

The S parameter mainly reflects annihilation with low-momentum valence electrons, whereas the W parameter is associated with high-momentum core electrons, providing information about the chemical environment surrounding the annihilation sites.

Because the S parameter represents an integrated fraction of counts in the central region, even subtle redistributions of counts within the annihilation peak can lead to measurable variations in S, although these changes may not be easily visible by direct inspection of the spectra. The S parameter, which is related to the low momentum of valence electrons, varies due to positron annihilation in the vacancy defects and within the free volume of the material. Variations of the S parameter have been widely reported in the literature as an indicator of changes in excess free volume within metallic glasses [36]. In contrast, the W parameter, which is related to the high momentum of core electrons, is sensitive to the chemical environment and varies with the presence of chemical defects. DBS measurements were conducted utilizing a high-purity germanium (HPGe) detector (Canberra GC2519) paired with a spectroscopic amplifier (ORTEC 572A) and a multichannel analyzer (ORTEC ASPEC-927).

Depth-dependent defect characteristics of the irradiated $Zr_{70}Ni_{30}$ alloy were investigated using DBS in combination with a variable-energy positron beam (VEPOS) system. The Doppler broadening line-shape parameters, S and the W, were determined with the SP-SE analysis software [37]. The S parameter was calculated by fixing the central region of the annihilation photopeak—calibrated against a Si reference sample—to a normalized width of 0.5, whereas the W parameter was obtained by defining the high-momentum wing regions with a constant value of 0.05.

Because the mean positron penetration depth is governed by the incident positron energy, monitoring the variation of the S parameter as a function of energy allows direct assessment of the depth distribution of open volume defects throughout the material. The mean positron implantation depth was estimated using the empirical relation [34, 38]:

$$\bar{z}(E) = \frac{40}{\rho} E^{1.6} \tag{1}$$

where $\bar{z}(E)$ represents the average implantation depth (nm), E is the positron energy (keV), and ρ denotes the material density (g cm^{-3}). This VEPOS–DBS methodology thus provides a powerful means of correlating energy-dependent Doppler parameters with defect profiles extending from the near-surface region into the quasi-bulk.

3. Results and discussion

3.1. Analysis of Doppler broadening spectroscopy data

The Doppler broadening spectra for the $Zr_{70}Ni_{30}$ metallic glass before and after Xe ion irradiation exhibit very similar spectral shapes at different positron incident energies, indicating that the irradiation induces only subtle modifications in the annihilation line shape. To avoid presenting crowded data and to improve clarity, the spectra obtained at a representative positron incident energy of 11 keV are shown. Furthermore, only the spectra corresponding to the unirradiated sample and the irradiated sample at a fluence of 2×10^{13}ionscm^{-2} are displayed in figure 3. This presentation allows the slight difference in the central part of the annihilation peak to be more clearly observed. Although the overall spectral shapes appear nearly identical, a small increase in the central region of the peak is visible for the irradiated sample. This subtle change corresponds to an increase in the fraction of low-momentum electrons contributing to the annihilation process and is quantified by the S parameter, which was extracted from the Doppler broadening spectra. Figure 4 presents six profiles of the S-parameter as a function of positron incident energy and the corresponding average depth for both non-irradiated and irradiated $Zr_{70}Ni_{30}$ TFMGs at different fluences. All the profiles are irregular at shallow depths (below 1keV, equivalent to an average penetration depth of about 5.54 nm) due to the diffusion of positrons

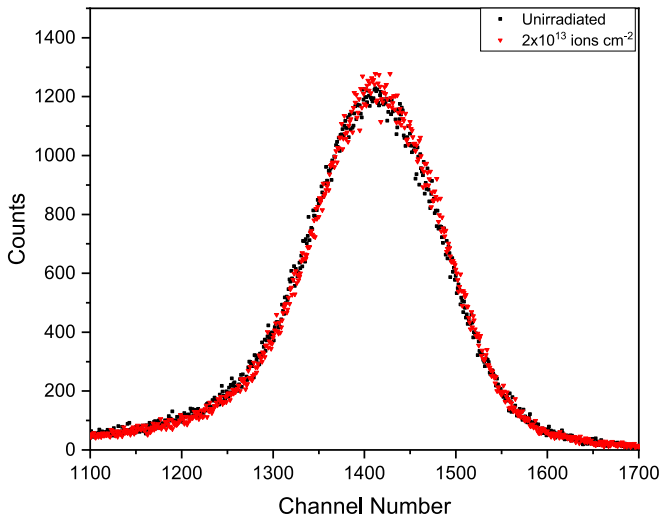

Figure 3. Doppler broadening spectra for unirradiated and Xe-irradiated $Zr_{70}Ni_{30}$ metallic glass at a fluence of 2×10^{13}ionscm^{-2}, obtained at a positron incident energy of 11keV.

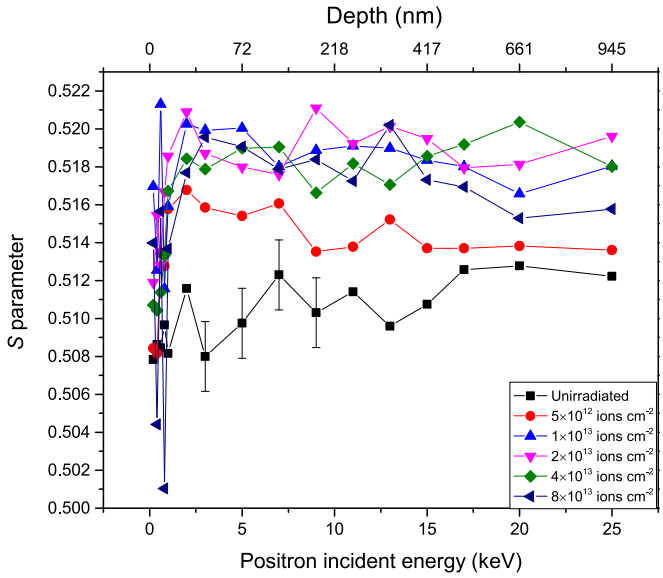

Figure 4. Evolution of the *S* parameter as a function of positron incident energy (keV) and corresponding depth (nm) for $Zr_{70}Ni_{30}$ metallic glass before and after Xe ion irradiation with different fluences. Error bars represent the standard deviation (0.0018) and are displayed only for selected points of non-irradiated sample to improve clarity, and are consistent with the other samples.

and their annihilation near the surface. However, with further increase in depth, all profiles gradually reach a plateau, where the *S*-parameter converge to stable values. This plateau indicates a homogeneous distribution of defects in the bulk region for all samples. The recorded profiles show a similar trend to those reported for the advanced metallic systems, such as high-entropy alloys [39]. The data collected within the positron energies above 1keV will be considered to describe the characteristics of annihilation positron-electron in the samples.

Compared to the as-deposited sample, the *S*-parameter of irradiated films increases with increasing ion fluence up to 2×10^{13} ions cm^{-2} while then displaying a slight decrease. The evolution of Doppler characteristics is more evident in figure 5, where the average values of the *S* parameter $\langle S\rangle$ are plotted as a function of the Xe ion fluence. Although the variation of the $\langle S\rangle$ parameter from $0.51\pm1.8\times10^{-3}$ in the unirradiated film to approximately $0.52\pm1.8\times10^{-3}$ in the film irradiated at 2×10^{13} ions cm^{-2} appears small, it is consistent with the expected sensitivity of positron annihilation spectroscopy to local atomic-scale changes in metallic glass. As the change is greater than the experimental error, the trend is considered significant, because the uncertainties are primarily governed by counting statistics due to the low repetition rate of the positron beam, resulting in relatively large error bars. Systematic errors, such as those arising from detector efficiency or instrumental drift,

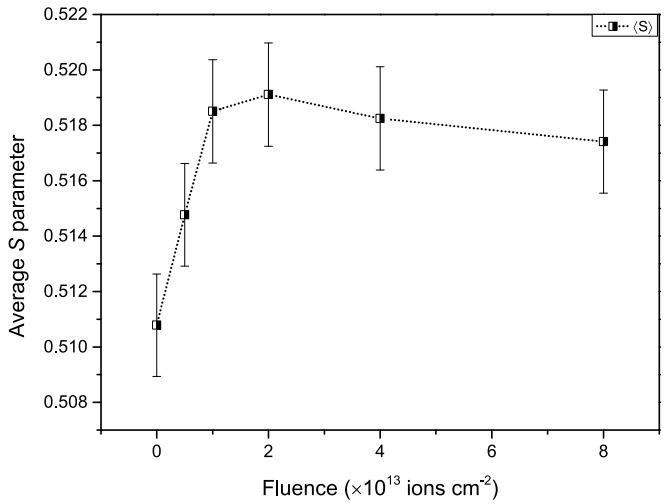

Figure 5. Evolution of the average *S* parameter ($\langle S \rangle$) as a function of irradiation fluence for $Zr_{70}Ni_{30}$ metallic glass. The short-dotted lines for guiding the eye. Error bars denote the standard deviation of repeated experimental measurements.

are effectively minimized because the analysis relies on ratios to determine the relative *S* parameter, which cancels many common systematic effects.

The slight increase in the $\langle S \rangle$ during the initial stages of irradiation can be explained by the generation of excess free volume in the irradiated films. A similar behavior has been found by Suo *et al* [25] in Fe-based MG under 28.8MeV Ne^{10+} ion irradiation. The subsequent slight decrease of the average *S*-parameter, when the fluence changes from 4×10^{13} ions cm^{-2} to 8×10^{13} ions cm^{-2}, presumably indicates a reduction of the amount of excess free volume. Qiu *et al* [40] reported that 3MeV Au^{2+} ion irradiation induced changes in excess free volume, which affected the mechanical properties of $Ni_{50}Nb_{10}Zr_{15}Ti_{15}Pt_{7.5}Cu_{2.5}$ MG. They demonstrated that the free volume generated at irradiation levels of 0.49 and 4.9 dpa can be annihilated when the dose is increased to 49 dpa, suggesting the formation of regions with local order. Furthermore, another study has demonstrated a good correlation between the increase of excess free volume and displacement damage generated by irradiation in amorphous alloys [41]. This relationship is particularly pronounced at low fluences, where structural changes in the irradiated thin film are primarily driven by an increase in excess free volume rather than by modifications of the glassy atomic configuration; the structure remains amorphous, as previously reported [28]. However, the accumulation of excess free volume during cascade collisions reaches a threshold due to saturation effects. As a result, it is possible that the local atomic arrangement relaxes into more stable configurations, thereby reducing the open volume available for positron annihilation. Such changes in excess free volume can significantly affect the *S* parameter, highlighting the relationship between the defects induced by swift heavy ion irradiation and structural relaxation mechanisms.

The slope of the *W* versus *S* curve serves as a fingerprint to identify the type of defects [40]. Therefore, to define these defects, the surface effect from the samples was removed based on the aforementioned data. Figure 6(a) illustrates the *W*-parameter as a function of the *S*-parameter , the error bars are hidden and shown mainly for the unirradiated sample to prevent clutter and to maintain clarity in the figure. The dotted black line is the linear fit of all data points, with a slope of (-0.48 ± 0.04). The linear correlation between the *S* and *W* parameters signifies the presence of a single type of open volume defects. In the present study, the data points (*S*, *W*) of samples irradiated at 5×10^{12}, 1×10^{13}, and 2×10^{13} ions cm^{-2} gradually shift towards higher values of the *S*-parameter and lower values of the *W*-parameter. They are distributed approximately around the fitted straight line, reflecting that a unique type of defect predominates in these samples. Suo *et al* [25] observed a similar distribution in the $Fe_{80}Si_7B_{13}$ MG irradiated at 4.6×10^{15} Ne cm^{-2}. As the irradiation fluence increases, the appearance of dispersed points below the fitted line suggests the presence of additional defect types, leads to a different mechanism of the positron annihilation process.

To clarify this point, we plotted the normalized average *W*-parameter ($\langle W \rangle / W_{uni}$) against the normalized average *S*-parameter ($\langle S \rangle / S_{uni}$), as shown in figure 6(b), where W_{uni} and S_{uni} denote the unirradiated reference values for both parameters. Two distinct slopes are clearly observed. The straight line represents the best correlation of the normalized data, exhibiting a negative slope at lower fluences ($\leqslant 2\times10^{13}$ ions cm^{-2}), which reveals the presence of an identical annihilation site where positron trapping occurs. This confirms that a single type of defect is present in each sample, and the three irradiated films exhibit the same evolution of excess free volume with different concentrations, reaching their minimum level at lower fluence (5×10^{12} ions cm^{-2}) and maximum level at a fluence of 2×10^{13} ions cm^{-2}. However, at high fluences ($>2\times10^{13}$ ions cm^{-2}), the normalized

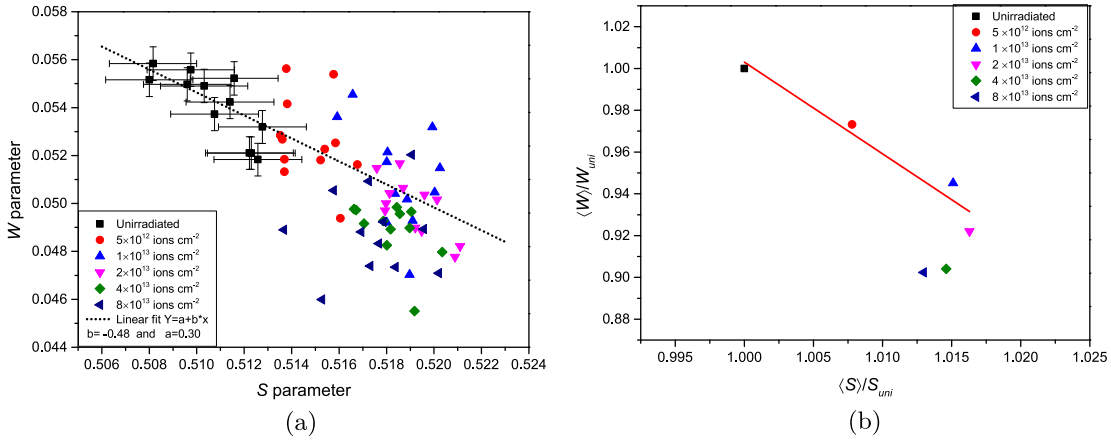

Figure 6. (a) Evolution of W as a function of S for unirradiated and irradiated $Zr_{70}Ni_{30}$ metallic glass with standard deviation shown. The short-dotted line indicates the linear fit to the data points. (b) Plot of the normalized average W-parameter ($\langle W\rangle/W_{\mathrm{uni}}$) versus the normalized average S-parameter ($\langle S\rangle/S_{\mathrm{uni}}$) for unirradiated and irradiated $Zr_{70}Ni_{30}$ metallic glass. The red line denotes the linear fit to the data [adj. $R^2 = 0.914$].

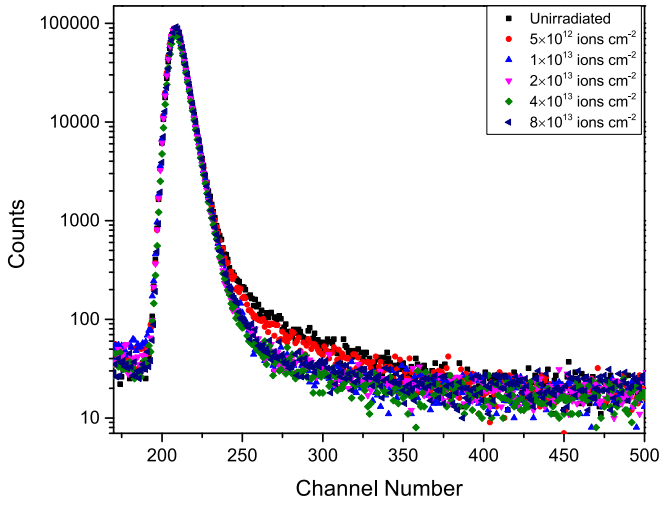

Figure 7. Positron annihilation lifetime spectra for $Zr_{70}Ni_{30}$ metallic glass before and after Xe ion irradiation.

data shift towards the bottom and to the left, with a significant change in slope, revealing the presence of a different type of defect. Flores *et al* [42] previously demonstrated that shifts in the distribution of the S-W points indicate that positrons annihilate at different annihilation sites, reflecting structural changes that could be associated with crystallization. In our case, the specimen exhibits significantly lower $\langle S\rangle$ and $\langle W\rangle$ values, indicating that positrons predominantly annihilate at different sites. This implies structural modifications that alters the nature of positron interactions, and these modifications can be associated with changes in the atomic arrangement and defect distribution along the swift heavy ions path. SRIM simulations demonstrate that the high energy deposition in the target $Zr_{70}Ni_{30}$ thin film is predominantly governed by electronic excitations (see figure 1). These excitations can result in localized heating and structural modifications, leading to ion-track formation via electron-phonon coupling [43]. Furthermore, point defects generated near irradiation tracks may reduce the free volume, further influencing positron annihilation characteristics.

3.2. Positron annihilation lifetime spectroscopy analysis

Figure 7 shows the positron lifetime (LT) spectra of $Zr_{70}Ni_{30}$ metallic glass before and after Xe ion irradiation. The deconvolution results of these PALS measurements are summarized in table 1.

The positron lifetime profile of the virgin $Zr_{70}Ni_{30}$ metallic glass consists of three components (τ_1,τ_2,and τ_3), each corresponding to positron trapping in different types of open-volume regions at the atomic scale. The presence of these three components (τ_1,τ_2,and τ_3) in the prepared sample is consistent with those reported for other metallic glasses [44, 45]. Similarly, Yang *et al* [2] reported three comparable lifetime components in a

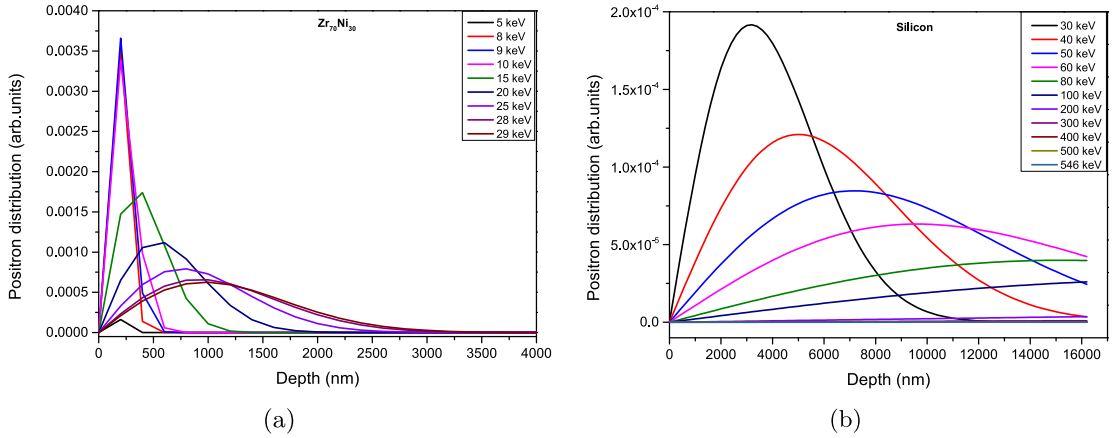

Figure 8. The mean positron implantation depth as a function of incident energy, calculated using Makhovian distribution for (a) $Zr_{70}Ni_{30}$ metallic glass and (b) silicon.

Table 1. Positron annihilation lifetimes components (τ_1, τ_2 and τ_3) with their associated intensities (I_1, I_2 and I_3) for the virgin and irradiated $Zr_{70}Ni_{30}$ metallic glass at different fluences.

Fluence (ions cm^{-2})	τ_1 (ns)	(I_1) (%)	τ_2 (ns)	(I_2) (%)	τ_3 (ns)	(I_3) (%)
0	0.150±0.001	36.8±0.4	0.272±0.001	61.3±0.4	1.92±0.04	1.90±0.03
5×10^{12}	0.148±0.002	31.1±0.4	0.271±0.001	67.5±0.4	1.93±0.05	1.45±0.03
1×10^{13}	0.148±0.002	25.5±0.6	0.257±0.001	73.9±0.6	1.70±0.08	0.690±0.032
2×10^{13}	0.151±0.002	23.9±0.2	0.2470±0.0004	75.9±0.2	1.77±0.05	0.588±0.022
4×10^{13}	0.151±0.001	26.1±0.2	0.253±0.001	73.3±0.2	1.66±0.05	0.680±0.022
8×10^{13}	0.154±0.001	26.4±0.2	0.2522±0.0004	72.8±0.2	1.49±0.04	0.768±0.022

binary metallic glass. The first component (τ_1) is the shortest lifetime, which is ascribed to the intrinsic micro-voids, similar to Bernal holes, located between regions of short-range atomic order. This component mostly reflects structural characteristics and includes contributions from para-positronium (p-Ps). The second lifetime component (τ_2) represents a combined signal from both the $Zr_{70}Ni_{30}$ thin film and silicon (Si) substrate. The positron lifetime in defect-free crystalline silicon has been experimentally determined to be approximately 0.220 - 0.230 ns. This range is consistent with experimental measurements and theoretical calculations reported in the literature [46]. However, the τ_2 values obtained in our measurements are significantly higher, ranging from 0.247 to 0.272 ns. The value of positron lifetime before irradiation (τ_2= 0.272 ns) exhibits strong concordance with the value of approximately 0.277 ns reported for $Zr_{52}Ti_6Al_{10}Cu_{18}Ni_{14}$ MG in previous research conducted by Vishwanadh *et al* [47]. Similarly, Flores *et al* [44] recorded that the τ_2 values are range from 0.268 to 0.371 ns for $Zr_{58.5}Cu_{15.6}Ni_{12.8}Al_{10.3}Nb_{2.8}$ metallic glass. These results confirm that the τ_2 lifetime originates from open-volume defects within the MG rather than from the Si substrate [46]. To further support these findings, the simulated positron implantation profiles for the $Zr_{70}Ni_{30}$ binary metallic glass and silicon were conducted using the Makhovian distribution function [48], defined as:

$$P(z,\,E) = \frac{mz^{m-1}}{z_0(E)^m}\exp\left[-\left(\frac{z}{z_0(E)}\right)^m\right]$$

Where m: the shape parameter depending on the material, z: the implantation depth and E: the energy of the incident positron. The parameter $z_0(E)$ depends on the incident positron energy (E) and is estimated using the following equation:

$$z_0(E) = \frac{40E^n}{\rho\,\Gamma\left(\frac{1}{m}+1\right)}$$

Where ρ: the density of the target material, n: a material-specific constant.

The resulting implantation profiles presented in figures 8(a) and (b), reveal that while a substantial number of positrons penetrate deeply into the silicon, a significant fraction is implanted at lower energies (< 29 keV) at nanometer-scale depths within the film. As the implantation energy increased above 29keV, majority of the collected information derives from the silicon substrate, while the near-surface regions of $Zr_{70}Ni_{30}$ thin film are notably sensitive to irradiation-induced defects. The presence of these defects enhances positron trapping,

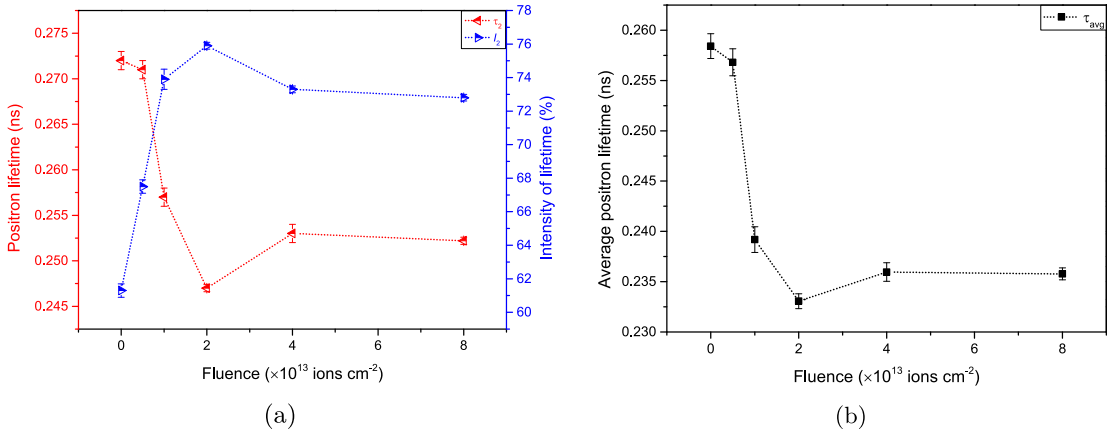

Figure 9. (a) Fluence-irradiation dependence of the lifetime component (τ_2) (red triangles) and the corresponding intensity (I_2) (blue triangles) for $Zr_{70}Ni_{30}$ metallic glass with the standard deviations, and (b) Variation of the average positron annihilation lifetime as a function of irradiation fluence for $Zr_{70}Ni_{30}$ metallic glass with the standard deviations. The short-dotted lines are interconnecting the data.

thereby prolonging the positron residence time and affecting the lifetime spectrum, mainly the τ_2 component and its corresponding intensity (I_2). Since the contribution of the positron lifetime from the Si substrate remains relatively constant, it can be inferred that the observed variation in the lifetime spectrum is mainly due to the irradiation-induced modifications in the $Zr_{70}Ni_{30}$ film. Therefore, the second lifetime (τ_2) is interpreted as a reflection of the excess free volume within the densely packed disorder structure of the MG. The τ_2 value of 0.272 ns, with an associated intensity of 61.3 % for the unirradiated specimen, demonstrates the incorporation of significant free volume within the prepared amorphous metallic glass. This is due to the sputtering method, which is a highly non-equilibrium deposition technique, producing materials with high free volume. These observations are consistent with the findings of Yavari *et al* [49], who demonstrated the presence of free volume in MGs. The τ_2 and I_2 evolution versus Xe ion fluence is presented in figure 9(a). As the ion irradiation fluence increases to 2×10^{13} ions cm^{-2}, τ_2 decreases from 0.272 ns to 0.247 ns, corresponding to a relative reduction of approximately 9 %, while I_2 increases from 61.3 % to 75.9 %, (24.8% increment), revealing an inverse relationship between these parameters. The increase in I_2 suggests a higher concentration of excess free volume, as more positrons are trapped within the irradiated thin film. This behavior is attributed to atomic displacements that create regions with low atomic packing density. Additionally, the decrease in τ_2 indicates a reduction in the average size of the excess free-volume sites, suggesting a redistribution of the excess free volume within the $Zr_{70}Ni_{30}$ metallic glass. Before irradiation, positrons in metallic glasses are predominantly trapped in pre-existing shallow open-volume regions [50]. However, high-energy ion irradiation generates more defects that serve as more effective positron traps compared to the original ones. Yang *et al* [2] reported that vacancy-like defects induced by irradiation in metallic glasses are unstable and tend to transform into extensive free volumes regions. Similar increases in the excess free-volume fraction have been observed in both experimental measurements and molecular dynamics simulations [51, 52]. Overall, at low fluences ($\leqslant2\times10^{13}$ ions cm^{-2}), swift heavy ion irradiation promotes a more uniform distribution of smaller free-volume sites within the $Zr_{70}Ni_{30}$ MG.

As the ion irradiation fluence increases to 4×10^{13} and 8×10^{13} ions cm^{-2}, both τ_2 and I_2 tend to reach a saturation level. Although τ_2 shows a slight increase at 4×10^{13} ions cm^{-2}, it remains below its initial value, reflecting an overall reduction of approximately 7%. Meanwhile, the intensity I_2 gradually decreases, probably due to a reduction of the density of open-volume defects. Hori *et al* [41], reported a significant reduction in free volume in $Zr_{50}Cu_{40}Al_{10}$ metallic glass irradiated by 2.5 and 200 MeV Xe ions at fluences of 1×10^{14} ions cm^{-2} and 1×10^{13} ions cm^{-2}, respectively, without inducing crystallization. This behavior is mainly attributed to structural relaxation. Similar relaxation behavior has been observed in Zr-based MG at irradiation dose of 4 dpa [53]. On the other hand, Nagel *et al* [54] reported a decrease in free volume of $Zr_{65}Al_{7.5}Ni_{10}Cu_{17.5}$ metallic glass during the annealing process, consistent with present findings. These results indicate that changes in defect concentration, rather than defect size, play a more significant role in determining the material properties and positron-trapping behavior under heavy-ion irradiation. At higher fluences, both parameters remain nearly constant, suggesting that a saturation threshold is reached and the positrons trapping are not significantly affected with additional irradiation fluence.

It is clear that the lifetime value (τ_2) is higher than the corresponding values noted in the literature for the bulk of both Zr and Ni (τ_{Zr}= 0.156 ns, τ_{Ni}= 0.096 ns). It also differs from the positron associated with mono-vacancies in the two metals (τ_{Zr}= 0.269 ns, τ_{Ni} = 0.169 ns) [55]. This suggests the absence of vacancy-like

defects in the irradiated films, likely due to the structural relaxation occurring after swift heavy ion irradiation. During this structural relaxation process, the vacancy-like defects generated by the collision cascades are unstable, and they are annihilated or transformed into large free volumes [2]. The last component (τ_3) represents the longest lifetime, characterized by the lowest intensity, and assigned to the lifetime of ortho-positronium (o-Ps). This appears when positrons are trapped in areas of low electron density, namely voids or holes formed during the preparation process [44]. Comparable values were observed by Flores *et al* [44]. As presented in table 1, both the third positron lifetime (τ_3) and its corresponding intensity (I_3) decrease considerably with increasing irradiation fluence. Specifically, τ_3 decreases from 1.92 ± 0.04 ns for the unirradiated sample to 1.49 ± 0.04 ns, while (I_3) drops from 1.90 ± 0.03 % to 0.768 ± 0.022 %. This reduction indicates changes in the distribution of density fluctuations within the disordered structure of the metallic glass, likely influencing both the size and the abundance of voids or holes. Moreover, the concentration (I_3) is negligible; hence, in the above discussion, we focused only on the data of τ_2 and (I_2), which describe the key characteristics of positron annihilation in $Zr_{70}Ni_{30}$ MG.

Figure 9(b) shows the variation of the average positron lifetime ($\tau_{avg}=\sum_i \tau_i I_i$, where τ_i and I_i are respectively, the positron lifetime associated with a specific type of open-volume defect i and its corresponding intensity) as a function of irradiation fluence. The τ_{avg} exhibits a trend similar to τ_2, indicating that the excess free-volume defects dominate the positron annihilation process. This evolution in τ_{avg} reflects a reduction in the concentration of the average open-volume defects. At higher irradiation fluence, τ_{avg} tends to stabilize, indicating a saturation state in the defect.

The comparison with the DBS results reveals that the intensity (I_2) exhibits behavior similar to that of S-parameter under xenon irradiation (see figures 5 and 9(a)). This correlation highlights the value of (I_2) as a complementary parameter to the S-parameter for evaluating the evolution of irradiation-induced excess free-volume. This suggests that $^{129}Xe^{23+}$ heavy-ion irradiation primarily affects the distribution and density of excess free-volume sites through rearrangements of atoms and relaxation processes within the thin film. The latter phenomenon can be attributed to a redistribution of the generated excess free volume, as previously reported by Egami *et al* [56]. In addition, the DBS analysis revealed other defects that may appear at high irradiation fluences. To confirm the current results, future research will focus on the use TEM analysis to investigate the formation and morphology of the additional defect structures.

4. Conclusion

In this investigation, the defect evolution of deposited $Zr_{70}Ni_{30}$ thin-film metallic glass after 93.2 MeV xenon heavy-ion irradiation at room temperature was examined using advanced positron annihilation spectroscopy techniques. At low fluences ($\leqslant 2\times10^{13}$ ions cm^{-2}), the S-parameter initially increased, and PALS analysis indicated a redistribution of free-volume sites and a reduction in their size, leading to modify of the short-range order distribution in $Zr_{70}Ni_{30}$ MG. At higher fluences (up to 2×10^{13} ions cm^{-2}), the S parameter, I_2 and τ_2 values decreased slightly and approached saturation. Furthermore, the S-W correlation analysis indicated a change in defect type above this fluence, suggesting the formation of additional irradiation-induced defects near the ion tracks. These findings demonstrate that the $Zr_{70}Ni_{30}$ thin film exhibits good irradiation tolerance, showing outstanding resistance to further defect accumulation beyond the fluence threshold.

Acknowledgments

We gratefully acknowledge the GANIL accelerator staff for Xe ion irradiations.

Data availability statement

All data that support the findings of this study are included within the article (and any supplementary files).

Funding

No funding was received for conducting this study.

Author contributions

Wafa Boukhemkhem 0000-0002-0346-3903
Conceptualization (equal), Data curation (equal), Formal analysis (equal), Investigation (equal), Methodology (equal), Writing – original draft (equal), Writing – review & editing (equal)

Rafik Hazem 0009-0000-2510-316X
Formal analysis (equal), Methodology (equal), Validation (equal), Writing – review & editing (equal)

Mahmoud Izerrouken 0000-0001-6750-3778
Conceptualization (equal), Project administration (lead), Supervision (equal), Visualization (equal)

Matteo Ghidelli 0000-0001-6057-9040
Resources (equal), Validation (equal), Writing – review & editing (equal)

Thomas Pardoen 0000-0003-0569-9466
Resources (equal), Validation (equal), Writing – review & editing (equal)

Saygin Kuzeci
Data curation (equal), Investigation (equal)

Murat Yavuz Yener
Data curation (equal), Investigation (equal)

Cumali Tav 0000-0002-6500-7903
Data curation (equal), Investigation (equal), Resources (equal)

Ugur Yahsi 0000-0002-6587-883X
Data curation (equal), Formal analysis (equal), Resources (equal), Writing – review & editing (equal)

References

[1] Xie Y *et al* 2024 Strengthening of Zr-based metallic glass at low dose helium ion irradiation *J. Nucl. Mater.* **592** 154943
[2] Yang L *et al* 2017 Structural responses of metallic glasses under neutron irradiation *Sci. Rep.* **7** 16739
[3] Zinkle S J and Was G 2013 Materials challenges in nuclear energy *Acta Mater.* **61** 735–58
[4] Okonkwo B O, Li Z, Li L, Wang J and Han E H 2025 Research progress on zirconium alloys: applications, development trend, and degradation mechanism in nuclear environment *Corros. Rev.* **43** 609–28
[5] Zinkle S J, Terrani K A, Gehin J C, Ott L J and Snead L L 2014 Accident tolerant fuels for LWRs: a perspective *J. Nucl. Mater.* **448** 374–9
[6] Tang C, Stueber M, Seifert H J and Steinbrueck M 2017 Protective coatings on zirconium-based alloys as accident-tolerant fuel (ATF) claddings *Corros. Rev.* **35** 141–65
[7] Kashkarov E, Afornu B, Sidelev D, Krinitcyn M, Gouws V and Lider A 2021 Recent advances in protective coatings for accident tolerant Zr-based fuel claddings *Coatings* **11** 557
[8] Luo W, Yang B and Chen G 2011 Effect of Ar^{+} ion irradiation on the microstructure and properties of Zr-Cu-Fe-Al bulk metallic glass *Scr. Mater.* **64** 625–8
[9] Ashby M and Greer A L 2006 Metallic glasses as structural materials *Scr. Mater.* **54** 321–6
[10] Wang W H 2012 The elastic properties, elastic models and elastic perspectives of metallic glasses *Prog. Mater. Sci.* **57** 487–656
[11] Ebner C, Rajagopalan J, Lekka C and Rentenberger C 2019 Electron beam induced rejuvenation in a metallic glass film during in-situ TEM tensile straining *Acta Mater.* **181** 148–59
[12] Xie G, Shao L, Louzguine-Luzgin D V and Inoue A 2011 He ion irradiation induced nanocrystallization in $Cu_{50}Zr_{45}Ti_5$ glassy alloy *Surf. Coat. Technol.* **206** 829–33
[13] Onodera N *et al* 2013 Irradiation effect of swift heavy ion for $Zr_{50}Cu_{40}Al_{10}$ bulk glassy alloy *Nucl. Instrum. Methods Phys. Res., Sect. B* **314** 122–4
[14] Zhang Z *et al* 2023 Ion irradiation effect on mechanical properties and corrosion resistance of a $Cu_{50}Zr_{50}$ metallic glass *Adv. Eng. Mater.* **25** 2101765
[15] Zhang H, Mei X, Wang Y, Wang Z and Wang Y 2015 Resistance to H^{+} induced irradiation damage in metallic glass $Fe_{80}Si_{7.43}B_{12.57}$ *J. Nucl. Mater.* **456** 344–50
[16] Huang P, Zhang S, Ren Y, Wang D, Qiu K and Wang J 2024 Temperature effect on the passivation of a novel Fe-based metallic glass in simulated wet storage environment of spent nuclear fuels *J. Mater. Sci.* **59** 16274–91
[17] Petrusenko Y, Bakai A, Borysenko V, Astakhov A and Barankov D 2009 Investigation of bulk metallic glass structure by means of electron irradiation *Intermetallics* **17** 246–8
[18] Li F, Liu X, Hou H, Chen G, Chen G and Li M 2009 Atomic scale calculation of the free volume in Zr_2Ni metallic glass *Intermetallics* **17** 98–103
[19] Brechtl J, Crespillo M L, Agarwal S, Bei H and Zinkle S J 2020 Effects of irradiation spectrum on the microstructural and mechanical properties of bulk metallic glasses *J. Nucl. Mater.* **533** 152084

[20] Bi R et al 2025 Research on the proton irradiation softening mechanism in Fe-based metallic glass coating Surfaces and Interfaces 58 105848
[21] Nagase T, Hosokawa T and Umakoshi Y 2005 Electron irradiation induced phase transformation in $Zr_{66.7}Cu_{33.3}$ and $Zr_{66.7}Pd_{33.3}$ metallic glass Scr. Mater. 53 1401–5
[22] Čížek J 2018 Characterization of lattice defects in metallic materials by positron annihilation spectroscopy: a review Journal of Materials Science & Technology 34 577–98
[23] Hruška P et al 2025 Investigation of microstructure and oxidation properties of amorphous and nanocrystalline HfNbTaTiZr high-entropy alloy thin films Surf. Coat. Technol. 496 131642
[24] Fukumoto Y, Ishii A, Iwase A, Yokoyama Y and Hori F 2010 Behavior of free volume in ZrCuAl bulk metallic glass after irradiation J. Phys. Conf. Ser. 225 012010
[25] Suo Y et al 2020 Study on the irradiation damage in Fe-based metallic glasses induced by Ne^{10+} ions Fusion Eng. Des. 157 111635
[26] Li N et al 2022 Effect on microstructure of $Fe_{80}B_{13}Si_7$ metallic glass irradiated by high intensity pulsed ion beam and He ions Surf. Coat. Technol. 449 128948
[27] Ghidelli M et al 2017 Homogeneous flow and size dependent mechanical behavior in highly ductile $Zr_{65}Ni_{35}$ metallic glass films Acta Mater. 131 246–59
[28] Boukhemkhem W et al 2023 Swift heavy ion irradiation effect on structural, morphological and mechanical properties of $Zr_{70}Ni_{30}$ metallic glass Phys. Scr. 98 085311
[29] Ghidelli M, Gravier S, Blandin J J, Pardoen T, Raskin J P and Mompiou F 2014 Compositional-induced structural change in Zr_xNi_{100-x} thin film metallic glasses J. Alloys Compd. 615 S348–51
[30] Ziegler J F, Ziegler M D and Biersack J P 2010 SRIM–The stopping and range of ions in matter Nucl. Instrum. Methods Phys. Res., Sect. B 268 1818–23
[31] Izerrouken M et al 2021 Heavy ion irradiation induced defects in Zircaloy-4 Phys. Scr. 96 045008
[32] Nallamothu R S et al 2024 Probing of CoO-induced nano-sized defects in Li_2SO_4–MgO–P_2O_5 glasses: insights from positron annihilation lifetime spectroscopy Physica B 690 416280
[33] Kansy J 1996 Microcomputer program for analysis of positron annihilation lifetime spectra Nucl. Instrum. Methods Phys. Res., Sect. A 374 235–44
[34] Jean Y, Mallon P E and Schrader D M 2003 Principles and Applications of Positron and Positronium Chemistry (World Scientific)
[35] Arrar A et al 2020 Optical and photoluminescence spectroscopy analysis and Doppler broadening annihilation radiation studies of perovskites based on $La_{1-x}Ni_xMnO_{2.75}$ thin layers Optik 224 165678
[36] Flores K M, Kanungo B P, Glade S C and Asoka-Kumar P 2007 Characterization of plasticity-induced structural changes in a Zr-based bulk metallic glass using positron annihilation spectroscopy J. Non-Cryst. Solids 353 1201–7
[37] Dryzek J (January 2024) SP-SE program available from the private website of Prof. Jerzy Dryzek at: https://ifj.edu.pl/private/jdryzek/page_r18.html
[38] Dahamni M E A et al 2026 Depth defect analysis of BaO thin films doped with Cd via positron annihilation techniques Phil. Mag. 1–13
[39] Hussain A et al 2023 Influence of defect dynamics on the nanoindentation hardness in NiCoCrFePd high entropy alloy under high dose Xe^{+3} irradiation Materials Science and Engineering: A 863 144523
[40] Qiu Y et al 2018 Mechanisms for the free volume tuning the mechanical properties of metallic glass through ion irradiation Intermetallics 101 173–8
[41] Hori F et al 2011 A study of defects in electron-and ion-irradiated ZrCuAl bulk glassy alloy using positron annihilation techniques J. Phys. Conf. Ser. 262 012025
[42] Flores K, Suh D, Dauskardt R, Asoka-Kumar P, Sterne P and Howell R 2002 Characterization of free volume in a bulk metallic glass using positron annihilation spectroscopy J. Mater. Res. 17 1153–61
[43] Rodriguez M et al 2012 Modification of Fe-B based metallic glasses using swift heavy ions EPJ Web of Conferences 35 03004
[44] Flores K, Sherer E, Bharathula A, Chen H and Jean Y 2007 Sub-nanometer open volume regions in a bulk metallic glass investigated by positron annihilation Acta Mater. 55 3403–11
[45] Su Y et al 2012 Bulk metallic glass formation: the positive effect of hydrogen J. Non-Cryst. Solids 358 2606–11
[46] Brusa R S, Deng W, Karwasz G and Zecca A 2002 Doppler-broadening measurements of positron annihilation with high-momentum electrons in pure elements Nucl. Instrum. Methods Phys. Res., Sect. B 194 519–31
[47] Vishwanadh B, Sharma S, Pujari P, Kishore R, Dey G and Tewari R 2013 Influence of free volume and medium-range order on the deformation response of rapidly solidified and bulk Zr-based ($Zr_{52}Ti_6Al_{10}Cu_{18}Ni_{14}$) metallic glass Phil. Mag. 93 3442–71
[48] Yabuuchi A, Tanaka M and Kinomura A 2020 Significant growth of vacancy-type defects by post-irradiation annealing in neon ion-irradiated tungsten probed by a slow positron beam J. Nucl. Mater. 531 152018
[49] Yavari A R et al 2005 Excess free volume in metallic glasses measured by x-ray diffraction Acta Mater. 53 1611–9
[50] Sugita K, Matsumoto M, Mizuno M, Araki H and Shirai Y 2008 Electron irradiation damage and the recovery in a Zr-based bulk amorphous alloy $Zr_{55}Cu_{30}Al_{10}Ni_5$ J. Phys. Conf. Ser. 106 012024
[51] Bian X et al 2016 Manipulation of free volumes in a metallic glass through Xe-ion irradiation Acta Mater. 106 66–77
[52] Avchaciov K, Ritter Y, Djurabekova F, Nordlund K and Albe K 2014 Effect of ion irradiation on structural properties of $Cu_{64}Zr_{36}$ metallic glass Nucl. Instrum. Methods Phys. Res., Sect. B 341 22–6
[53] Sun K et al 2020 Structural rejuvenation and relaxation of a metallic glass induced by ion irradiation Scr. Mater. 180 34–9
[54] Nagel C, Rätzke K, Schmidtke E, Faupel F and Ulfert W 1999 Positron-annihilation studies of free-volume changes in the bulk metallic glass $Zr_{65}Al_{7.5}Ni_{10}Cu_{17.5}$ during structural relaxation and at the glass transition Phys. Rev. B 60 9212
[55] Robles J C, Ogando E and Plazaola F 2007 Positron lifetime calculation for the elements of the periodic table J. Phys.: Condens. Matter 19 176222
[56] Egami T 1978 Structural relaxation in amorphous $Fe_{40}Ni_{40}P_{14}B_6$ studied by energy dispersive x-ray diffraction J. Mater. Sci. 13 2587–99